SCIENCE CHINA
Technological Sciences

May 2011 Vol.54 No.5: 1154–1168
doi: 10.1007/s11431-011-4360-x

Vibrational characteristics of piping system in air conditioning outdoor unit

S. K. LOH[1], W. F. FARIS[2*], M. HAMDI[1] & W. M. CHIN[3]

[1] *Department of Engineering Design & Manufacture, Faculty of Engineering, University of Malaya, 50603 Kuala Lumpur, Malaysia;*
[2] *Department of Mechanical Engineering, College of Engineering, International Islamic University Malaysia, 50728 Kuala Lumpur, Malaysia;*
[3] *O.Y.L. R&D Sdn Bhd, Sungai Buloh, Selangor Darul Ehsan, Malaysia*

Received January 8, 2011; accepted February 21, 2011; published online March 31, 2011

The modal analysis of piping system in air conditioner (AC) outdoor unit is essential to investigate the vibration properties of the system. In view of the growing significance of numerical finite element (FE) model for vibration behaviour prediction, the AC piping elastic end support characterization has been explored. The axial and radial stiffness variables (k_a, k_{r1}, k_{r2}) of the compressor-piping mounting are obtained and represented by dynamic stiffness of compressor grommet. They are obtained from dynamic load deflection test based on compressor operating condition such as excitation frequency and amplitude. The unknown stiffness variables of the other tube end (chassis-piping mounting) are determined by parameter fine tuning. An experimental modal analysis using impact hammer test has also been employed to determine the vibration properties such as natural frequencies, mode shapes and damping ratio of the piping structures. The modal parameters acquisition using SCADAS mobile acquisition system and LMS Impact Testing software is compared with the corresponding simulated modal properties using Abaqus. Most of the simulated natural frequencies achieve good correlation with the measured frequencies and it is reasonably a good prediction model to predict vibration behaviour of AC piping structures.

air conditioning outdoor unit, piping, modal analysis, vibration characteristics

Citation: Loh S K, Faris W F, Hamdi M, et al. Vibrational characteristics of piping system in air conditioning outdoor unit. Sci China Tech Sci, 2011, 54: 1154–1168, doi: 10.1007/s11431-011-4360-x

1 Overview

Piping structures of air conditioner outdoor unit especially discharge and suction pipes shown in Figure 1 are vibration prone structures and they are always excited by mechanical excitation of compressor and fluid flow pulsation. Excessive vibration of the pipelines can lead to structural damage and fatigue. It may cause structural-borne acoustic problem and then give annoyance to end users. Therefore, it is in the first place significant to study the fundamental vibration characteristics of the pipes before the effort to characterize the forced vibration.

The vibration properties simulated by finite element (FE) approach have been becoming a fundamental and essential method during the structural design process. Even though the frequency extraction procedure using FE computational tool is simple and straightforward, the accuracy of the vibration behaviour depends much on the boundary condition specified to the structure, provided no significant deviation is found on the material properties. In this work, the elastic support characterization for the compressor-pipe mounting has been performed on the compressor rubber isolator using dynamic load deflection test. The stiffness characterization is being established and applied to the piping models, with the elastic support at the chassis-pipe mounting being de-

*Corresponding author (email: waleed@iiu.edu.my)

© Science China Press and Springer-Verlag Berlin Heidelberg 2011

termined by fine tuning based on impact hammer test. Figure 2 shows the vibration characteristics of AC outdoor pipelines which can be determined by impact hammer test and verify the finite element model with defined elastic supports.

Modal analysis is the study of the dynamic properties of structures under vibration excitation. It provides a set of modal parameters that characterize the dynamic behavior of a structure. For empirical approach, it is often called Experimental Modal Analysis as it is a field of measuring and analyzing the dynamic response of structures when excited by an input. For instance, when a structure is subjected to an input force, the most common data of frequency response function (FRF) can be obtained before the estimation of modal parameters is applied. In general, the modal parameters such as frequency, mode shapes and damping are estimated using parameter estimation methods. These modal parameters form the modal model. The corresponding relation for measured data FRFs is given in as follows [1]:

$$h_{ij}(j\omega)=\sum_{k=1}^{N}\left[\frac{r_{ijk}}{(j\omega-\lambda_k)}+\frac{r_{ijk}^{*}}{(j\omega-\lambda_k^{*})}\right], \tag{1}$$

where $h_{ij}(j\omega)$ is the FRF between the response DOF i and reference DOF j ; N is the number of modes of vibration that contribute to the structure's dynamic response within the frequency range under consideration; r_{ijk} is the residue value for mode k; λ_k = pole value for mode k; * designates complex conjugate.

The pole value can be expressed as

$$\lambda_k=\delta_k+\mathrm{j}\omega_{dk}, \tag{2}$$

where ω_{dk} is the undamped natural frequency of mode k; δ_k is the damping factor of mode k,

or

$$\lambda_k=-\zeta_k\omega_{nk}+j\omega_{nk}\sqrt{1-\zeta_k^{2}}\,, \tag{3}$$

where ω_{nk} is the undamped natural frequency of mode k; ζ_k is the damping ratio of mode.

The residue value is the product of three terms

$$r_{ijk}=a_k v_{ik} v_{jk}, \tag{4}$$

where v_{ik} is the mode shape coefficient at response DOF i of mode k; v_{jk} is the mode shape coefficient at reference DOF j of mode k; a_k is a complex scaling constant, whose value is determined by the scaling of the mode shapes.

Free vibration research works and efforts have been widely known and conducted in Finite Element Method (FEM) and Modal Testing. Chuan-xue Duan and Guang Meng [2] determined the boundary condition of the air conditioner piping system using the rotational degree of freedoms (RDOFs) component mode synthesis (CMS) method. The RDOFs were estimated from the measured translational degree of freedoms (TDOFs) and the boundary condition described by mass, damping and stiffness matrices were obtained by estimating RDOFs CMS method. The CMS method was used to describe the components of piping system in dynamic analysis and yield the related matrices based on the measured RDOFs. The complex boundary condition of the FE piping models was determined for frequency extraction. Although the FE analysis results are comparable with experimental results, there appear some frequencies in FE which do not appear in experiment. Wang et al. [3] employed FEM to predict the free vibration and buckling characteristics of complete circular toroidal shells with meridional ring stiffeners. Results for the natural frequencies and the critical buckling pressure were obtained for shells covering a wide range of the geometric parameters. The results compared well with previously published results. Pan et al. [4] investigated the vibration characteristics of ring stiffened cylinders associated with arbitrary boundary conditions by using the exponential functions and axial factors. Both analytical and numerical researches proved that when the axial factor is a pure imaginary number, the cylinder appears to have a certain length with shear diaphragm boundary conditions.

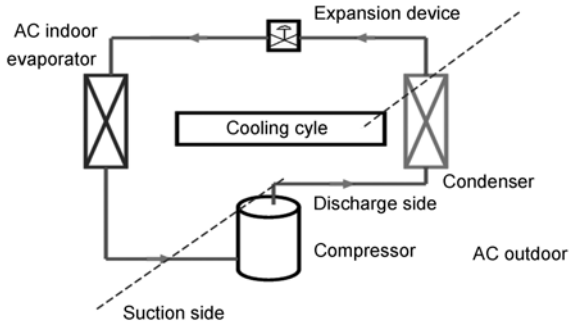

Figure 1 Discharge and suction tubes mounting to compressor.

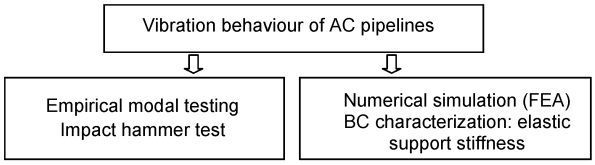

Figure 2 Elastic support stiffness characterization for elastic boundary condition in finite element model.

2 Impact hammer testing

An impact hammer test has been performed on 2 pipeline structures of a 2-HP air conditioner outdoor unit. The pipelines are suction tube assy and discharge tube assy. Figure 3(a) shows the internal piping structures of the air conditioner outdoor unit. To perform the modal impact test, the equipment, such as an ICP tri-axial accelerometer, an impact hammer, a SCADAS Mobile Data Acquisition System

(DAQ) and a modal testing software known as LMS Test Lab: Impact Testing and Modal Analysis is employed to measure the Frequency Response Function (FRF), phase and coherence of the structure. Figure 3(b) shows the experimental setup of modal impact hammer test.

The geometry of the pipeline is being import into the Test Lab Impact Testing geometry workbook and set as wireframe model in the software. Before measurement, some setup such as channel setup, calibration, impact scope and impact setup need to be configured. In channel setup, the impact hammer and accelerometer are connected to the appropriate front end channels in the DAQ. The direction of the hammer and accelerometer need to be correctly set to match the axis in the geometry display. The equipment such as accelerometers and impact hammer is required to be calibrated in a calibrator to determine its sensitivity. The measured sensitivity is applied in the impact test for measuring signal response accurately. In impact scope, the input force range is set as optimal as possible to ensure the impact signal is visible and distinctive.

Impact setup configures the triggering level, bandwidth, windowing and driving points. In general practice, the trigger settings are automatically set based on a few hits. Based on the input force, a minimum force level is set as the triggering level for the impact force during measurement. The bandwidth and spectra resolution of the measurement are also specified to acquire the frequency of interest and the resolution of data. The sampling frequency f_s is normally set similar to the bandwidth but it is ideally set twice the bandwidth frequency f_{max}:

$$f_{max} = 2 \times f_s, \tag{5}$$

The frequency resolution D_f is shown as below:

$$D_f = \frac{1}{T}, \tag{6}$$

where T is the observation time. The finer the desired frequency resolution D_f, the longer the acquisition time T. The windowing is also applied to the input and response. In general the common exponential window is applied to the input force and response. The application of windowing reduces the signal amplitude to zero at the end of the acquisition time to ensure no signal leakage over the frequency range.

The impact points of Suction Tube Assy and Discharge Tube Assy structures are located at about 30 and 60 impact points respectively and the output signal measurement is taken using accelerometer on a driving point with high mobility. The impact and accelerometer measurement points are indicated in Figure 4. The measurement point of suction tube is located at Point-15 while the measurement point of discharge tube is at Point-17.

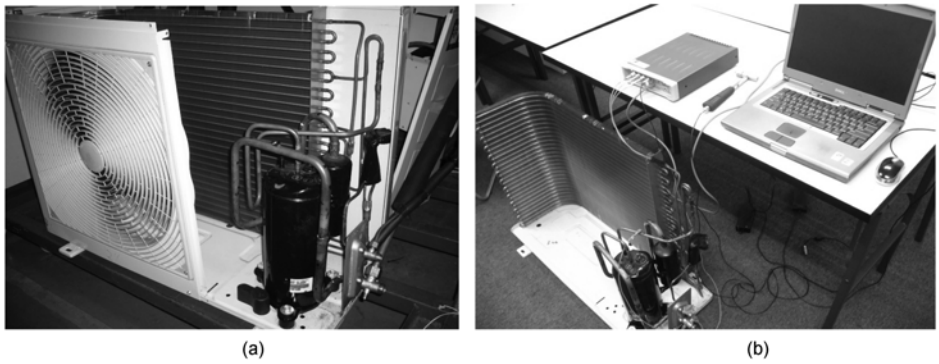

Figure 3 (a) Suction and discharge tubes in air conditioner outdoor unit mounting to their adjacent parts; (b) equipments setup of modal impact hammer test.

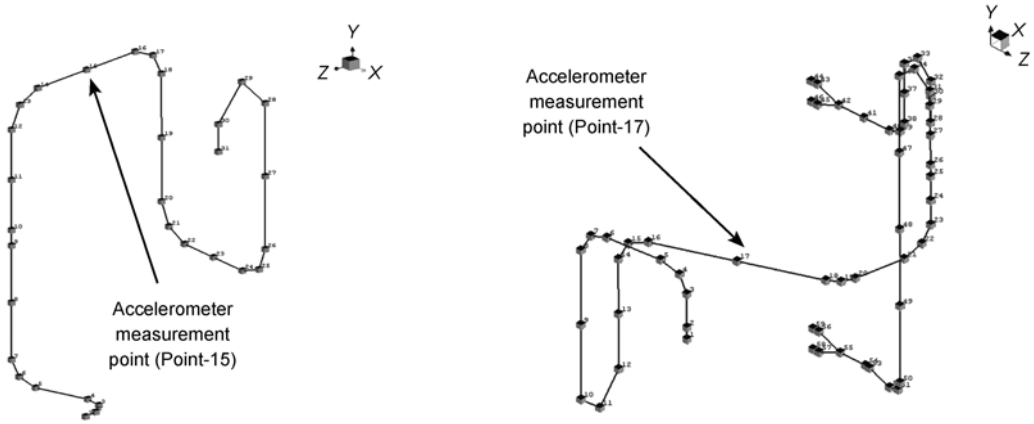

Figure 4 Impact points on the suction and discharge tube assy with measurement driving point at Point-15 and Point-17 respectively.

After the specimen and program setup have been completed, the impact hammer test can be performed on the structures. An accelerometer is placed on the designated measurement point of the pipe. The bottom surface of the accelerometer is applied evenly with adhesive in order to fix the accelerometer on the pipe. The setting in LMS Test Lab: Impact Testing is then configured before the acquisition process is started. The initial frequency bandwidth of interest is set as 200 Hz. The impact hammer is used to hit the first impact point i.e. Impact Point-1 and ensure an impulse is generated. The input energy needs to be distributed over the frequency range. The hit is repeated for 5 times for data averaging purpose. After the measurement of first impact point is done, move on to the rest of the impact points and repeat the impact process again. The frequency bandwidth is changed to 40 Hz and the process is repeated for low frequency range investigation. The tip of the impact hammer may need to be changed to the softer type so that sufficient input energy is excited over a small frequency range.

2.1 Modal impact test results

The frequency bandwidth of 30–40 Hz investigates the FRF profiles in the low frequency range while the bandwidth of 200 Hz presents the picture of FRF profiles in a wider frequency range. The frequency response function (FRF) and coherence of the suction tube assy and discharge tube assy are shown in the Figures 5 to 9.

The peaks on the FRF plots of each point are the eigenvalues of the system which correspond to the natural frequencies. The summation of FRF integrates all the FRF data measured in each point and it is distinct to extract natural frequencies in the particular frequency range. The coherence shows the contamination level of the FRF data and good FRF data contains coherence near to 1. The potential natural modes are investigated and correlated with coherence data to examine the validation of the selected modes. The measured natural frequencies of the suction tube assy and discharge tube assy are tabulated in Tables 7 and 8.

3 Modal parameters prediction using finite element (FE) simulation

To determine the fundamental inherent characteristic property of the pipeline structures, the finite element (FE) numerical tool can also be used. The eigenvalue problem for the natural frequencies of an undamped finite element model is [5]:

$$(-\omega^2 M^{MN} + K^{MN})\phi^N = 0, \tag{7}$$

where M^{MN} is the mass matrix which is symmetric and positive definite; K^{MN} is the stiffness matrix, which includes initial stiffness effects if the base state included the effects of nonlinear geometry; Φ^{N} is the eigenvector or mode of vibration; M and N are degrees of freedom.

In this research project, the FE software called Abaqus Standard has been employed to predict the natural responses of the structures. The frequency extraction procedure performs eigenvalue extraction to calculate the natural frequencies and the corresponding mode shapes of a system.

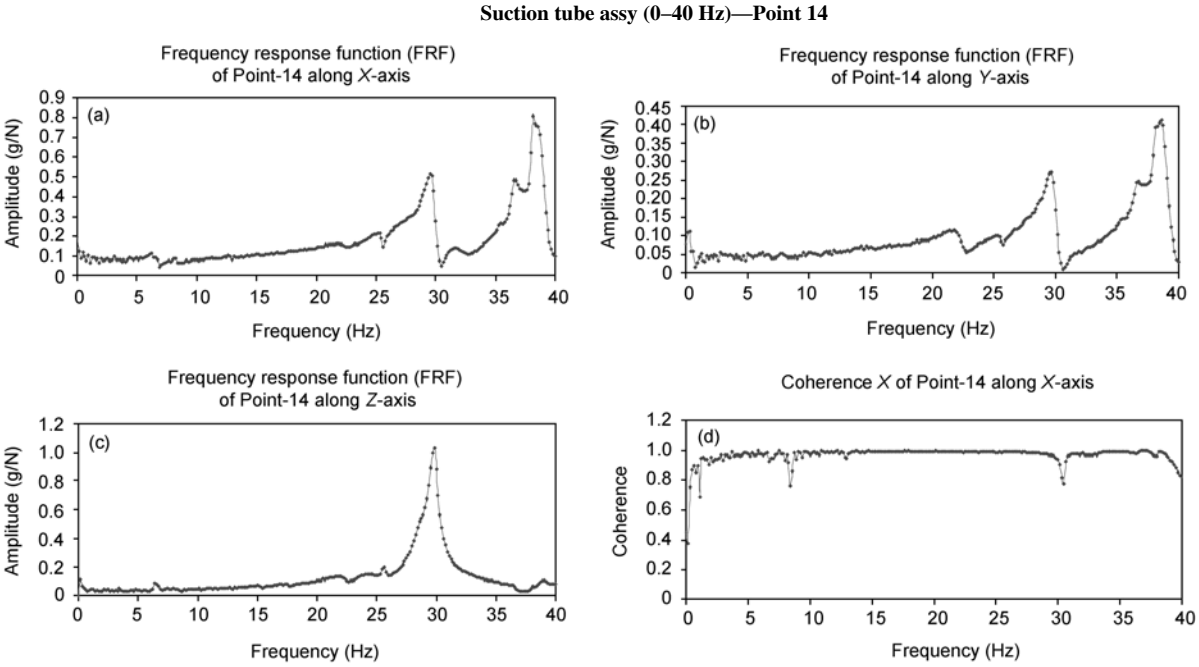

Figure 5 FRF along *X*, *Y*, *Z* axes and coherence plot of suction tube assy Point 14.

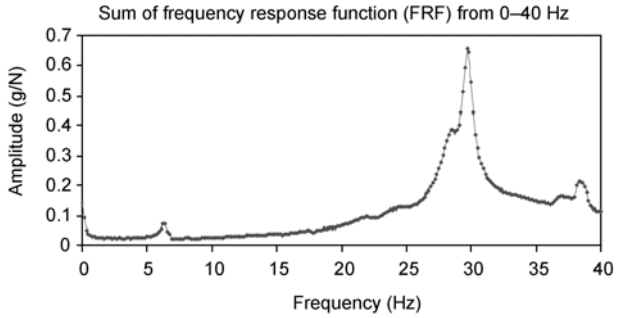

Figure 6 FRF summation of suction tube assy for frequency range 0–40 Hz.

Two main eigenvalue extraction methods available in Abaqus Standard are Lanczos and Automatic multi-level substructuring (AMS). The Lanczos extraction has been employed in this work.

3.1 The model

To minimize the computational consumption, all the two simulation piping models have been meshed with shell elements. The simulation is using the actual pipe geometry assigned with shell elements and a thickness is assigned to the shell elements. The thickness of suction tube and discharge tube are 1.2 and 0.8 mm respectively. As the material used is copper-phosphorus alloy, the material property particularly elasticity modulus is obtained from the tensile test on the material specimens and they are tabulated in Table 1 below. The density is calculated from the physical mass of the pipeline.

Table 1 Material properties of copper alloy C1220T

Material properties	Value
Young's modulus (GPa)	26.84
Density (tonne/mm^3)	8.946×10^{-9}
Poisson's ratio	0.343

For the boundary condition, all the pipe ends mounted to the compressor, accumulator, condenser coil etc. can be moved at a different degree due to the constrain condition of the adjacent connecting parts. Therefore, the pipe ends are defined as elastic supports. To define the movement of the pipel ends, different axial and radial stiffnesses needs to be defined in the model. The suction tube assy model includes the main suction from valve spanning to the accumulator. The connecting mass of accumulator is included and represented as a point mass in the model. The axial and radial stiffnesses are being defined beyond the point mass and the other pipe end.

For the discharge tube assy model, the discharge pipeline spans from the compressor to the condenser coil with the compressor point mass being added as connecting mass. The stiffness is defined at both the pipe ends. Figure 10 shows the suction tube assy and discharge tube assy models in shell elements. As the models are not complex with less than 1 million DOFs, the Lanczos eigensolver has been applied to extract the eigenvalues and the corresponding eigenvectors for the frequency range up to 200 Hz. Figure 11 shows the modeling of connecting mass and spring stiffness to the copper tube.

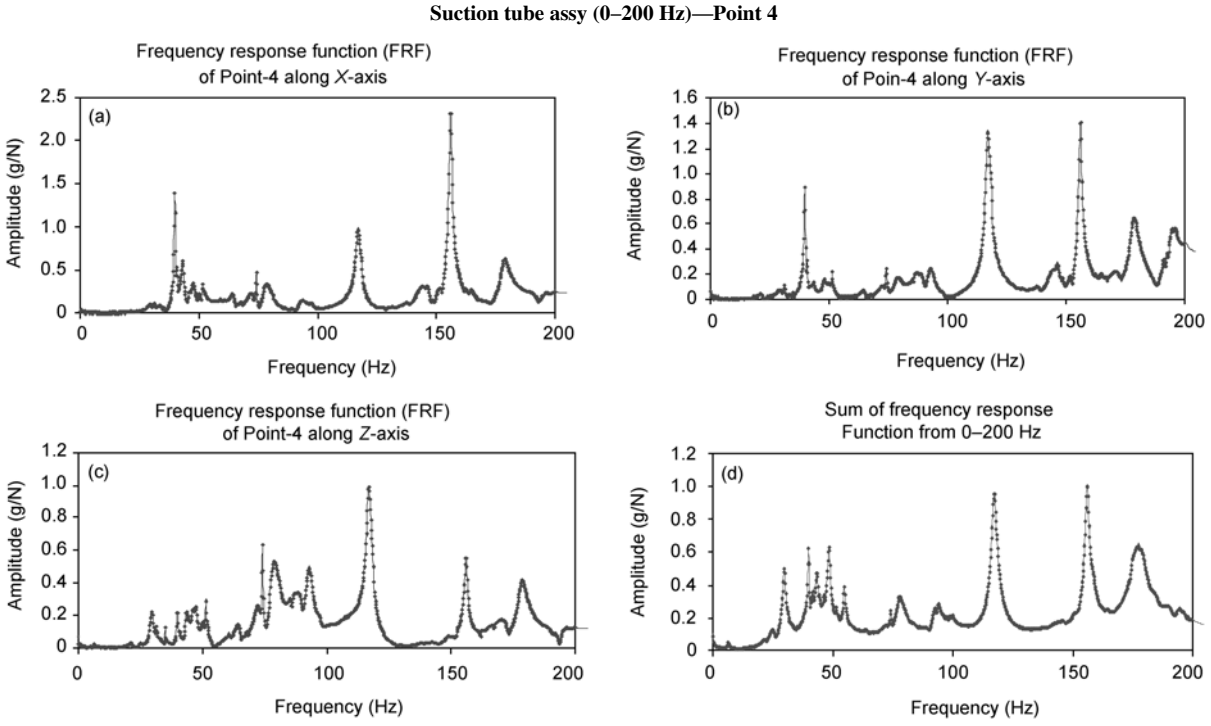

Figure 7 FRF of suction tube assy Point 4 along *X*, *Y*, *Z* axes and its FRF summation for frequency range 0–200 Hz.

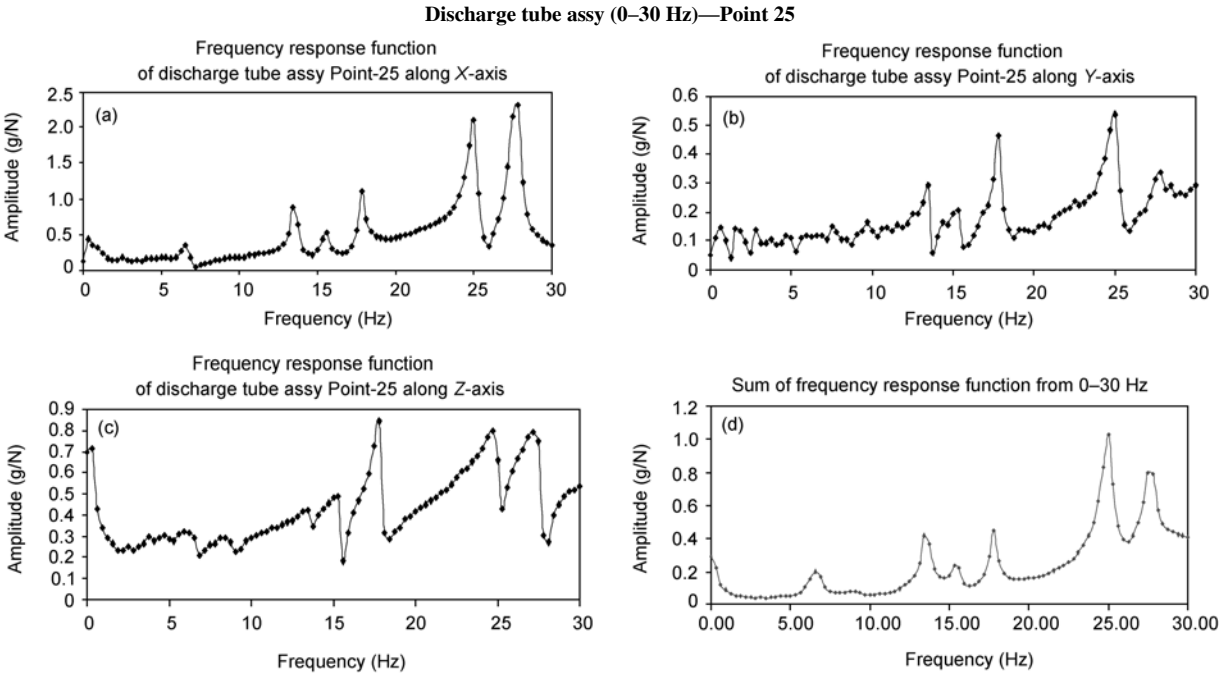

Figure 8 FRF of discharge tube assy Point 25 along *X*, *Y*, *Z* axes and its FRF summation for frequency range 0–30 Hz.

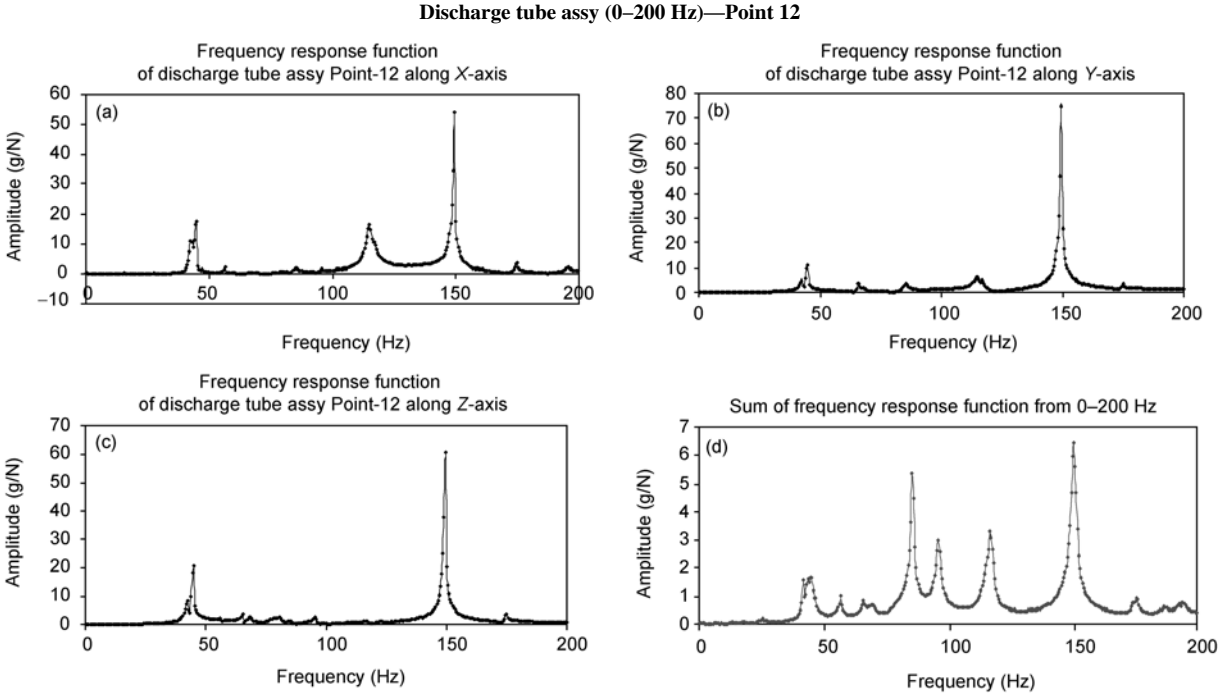

Figure 9 FRF of discharge tube assy Point 12 along *X*, *Y*, *Z* axes and its FRF summation for frequency range 0–200 Hz.

3.2 Investigation of fully constraint structure, mesh density and element types to optimal modal characteristics

In view of the predetermined boundary stiffness, this section involves case study to determine the natural frequency of the fully constraint structure. Under the full translational and rotational constraint, higher frequency is predicted and the material properties take significant effect in determining the natural characteristics.

There are mainly two types of shell element in Abaqus Standard, categorized as finite strain and small strain shell elements. The finite strain element accounts for finite membrane strains and arbitrarily large rotation and the small strain element provides for arbitrarily large rotations but

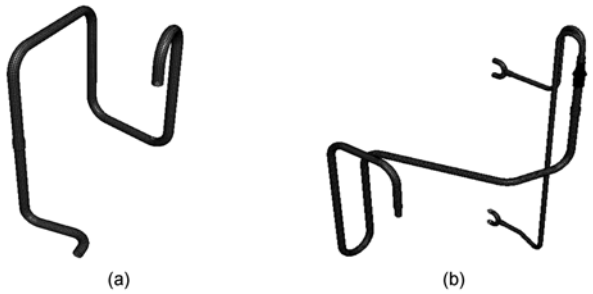

Figure 10 Suction and discharge tube assy in shell elements environment. (a) Suction tube; (b) discharge tube.

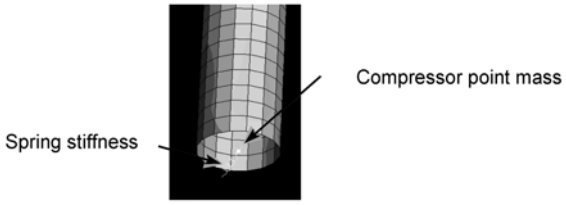

Figure 11 Component (compressor) mass and spring stiffness modeling shot in FEA.

only small strains. A study on the difference between the finite strain element and small strain element has been conducted to investigate the effect of two different shell element on the overall natural characteristics of the pipelines.

Besides, a different structural mesh density has been performed to examine the variation possibility of natural frequency. Primary prediction assumes that no frequency variation will be expected as the mesh density does not contribute to the mass and stiffness of the system. The first-order element type is selected as it is computationally economic and gives accurate result in frequency analysis. This is a common practice and in line with the finite element method (FEM) recommended by Nitin [6]. Table 2 shows the natural frequencies of the suction tube assy under full boundary constraint, two different mesh densities and shell element types.

Based on the investigation, the element type of finite strain and small strain and different mesh density apparently do not present much difference to the natural characteristic of free vibration. For optimal resources while retaining the smoothed geometry profile, the regular first order finite membrane shell S4 with element size of 3 mm is finally opted for frequency analysis.

3.3 Determination of system stiffness for modal testing correlation

The determination of stiffness of pipeline system is rather complicated in the manner of involving the measurement of pipe end deflection subjected to an applied force. It is one of the two main properties to determine the system natural frequencies. As the three translational degree of freedom (DOF) stiffness exists at each pipe end, it is found tremendously difficult to determine the real stiffness by measurement. In view of many unknown support stiffness existing in the system, effort to find stiffness of the compressor-piping mounting has been performed to minimize the number of unknown stiffnesses. The rubber grommets sat between the base panel and the compressor control the movement DOF of the compressor. Therefore, the grommet is tested to determine its axial and radial stiffnesses as a representation of axial and radial stiffnesses of compressor-piping mounting. The remaining unknown stiffness is applied by fine tuning in the simulation model until correlation with experiment data is reached. Figure 12 briefs the method used to predict the elastic support stiffness for the FE model.

Table 2 Natural frequency comparison of fully constraint copper suction tube using different element type and mesh densities[a)]

Mode	Finite mem brane strain (S4); ES3.0	Small membrane strain (S4R5); ES3.0	Finite membrane strain (S4); ES0.5
1	18.86	18.79	18.96
2	22.87	22.76	22.91
3	26.88	26.73	26.79
4	45.89	45.76	46.24
5	58.59	58.33	58.65
6	90.23	89.78	90.42

a) Abbreviation: Element Size = ES.

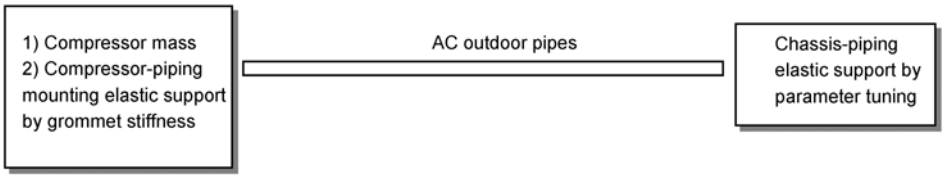

Figure 12 Elastic support characterization and fine tuning in FE model.

3.3.1 Determination of rubber grommet stiffness

In air conditioner piping vibration, the rubber grommets placed below the compressor are deflected in the same situation and acts to isolate vibration.

Typically, there are two types of stiffnesses—static and dynamic stiffnesses. The determination of the static and dynamic stiffness characteristics becomes critical to the function of the product. Generally, the dynamic stiffness is higher than the static stiffness. As vibration is a dynamic phenomenon and normally involves relatively large displacement, the rubber isolation especially highly damped isolator is dependent upon the behaviour of the rubber grommet under dynamic operating condition [7]. Since rubber isolator has rate dependent stiffness property [8], it is appropriate to characterize the property at the actual dynamic condition in order to predict the system vibration characteristics. The rubber grommets used in the analyzed outdoor unit are EPT rubber and the information of stiffness is not provided by the supplier. Hence the static and dynamic load-deflection tests are conducted to identify the static and dynamic stiffnesses of the rubber.

a) Static load deflection test

A static load deflection test is considered 'static' when the loading rate or compression rate is low. Basically there is no specification or high restriction on the rate but preferably it shall be controlled not exceeding 0.8 mm/s in deflection rate. The radial and axial load deflection measurements have been performed based on the load and displacement rate control. A load machine MTS 830 Servo-Hydraulic Elastomer Testing Machine with capacity 10 kN/ $\pm$25 mm is used to perform and static and dynamic load deflection test. Figure 13 shows the test setup to perform the tests.

Figure 14(a) shows the static radial load against deflection curves. It is found that the test with compressive loading rates of 6.7 and 3.3 N/s give 2 gradient curves close to each other. Therefore, the yielded radial stiffnesses are close to each other, i.e., approximately 11.6–12 N/mm. The compressive loading rate applied in the test is not significant to affect the load-deflection gradient linearly but slightly increase the curve gradient of higher compressive loading rate when the grommet deforms in a non linear condition. When the test input parameter is changed to deflection rate of 0.5 mm/s and controlled to a maximum compression linear region of about 3 mm, it corresponds to a higher compressive loading rate, yielding higher radial stiffness as shown in Figure 14(b). When the compressive loading rate is higher, this corresponds to a higher stiffness. Based on the data, the grommet is subjected to linear deformation initially and followed by nonlinear deformation. The static radial and axial stiffness values are tabulated in Tables 3 and 4.

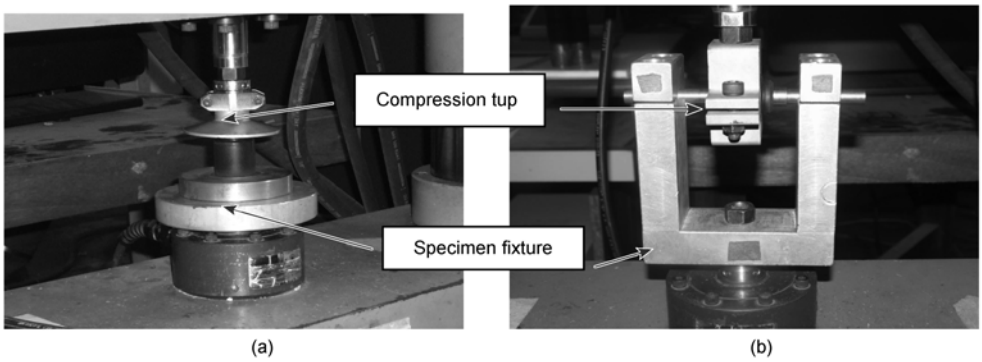

Figure 13 The setup of rubber grommet for (a) axial and (b) radial stiffness characterization.

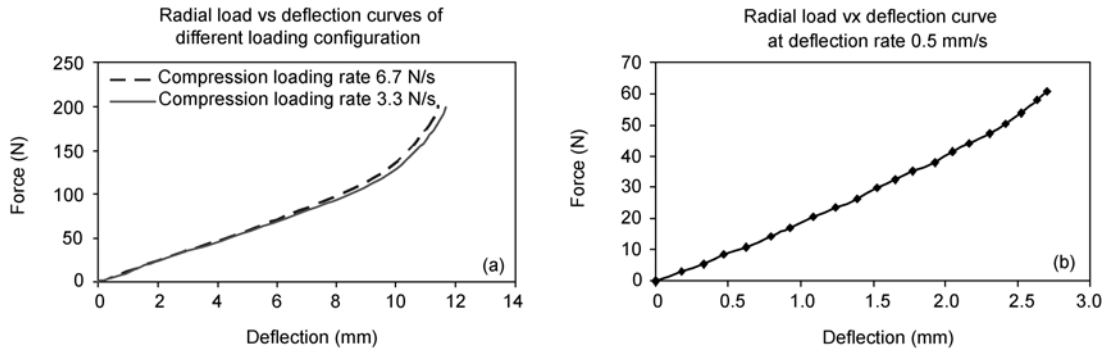

Figure 14 Radial load-deflection curves at (a) different loading rates and (b) deflection rate 0.5 mm/s.

Table 3 Static radial stiffness of rubber grommet in linear region

Sample No.	Test configuration	Static radial stiffness (N/mm)
1	loading rate 6.7 N/s	12.0
2	loading rate 3.3 N/s	11.6
3	deflection rate 0.5 mm/s	20.0

Table 4 Static axial stiffness of rubber grommet in linear region

Sample No.	Test configuration	Static axial stiffness (N/mm)
1	loading rate 6.7 N/s	61.1
2	loading rate 3.3 N/s	60.5
3	deflection rate 0.5 mm/s	87.5

The axial load-deflection of the grommet shown in Figure 15 happens much in a non linear condition as the linear deformation occurs up to 0.6 mm. Beyond this displacement, the grommet undergoes non linear deformation. It is apparent that the grommet is stiffer in the axial direction due to stiffer grommet design along the axial direction. Grommet is relatively low in stiffness along the radial direction as the grommet is hollow in the middle inside. Hence, this results in a higher axial stiffness.

b) Dynamic load deflection test

As the rubber grommet generally isolates vibration under dynamic operating condition of the system, its applications are dependent upon the dynamic behaviour of the rubber. The dynamic loading is applied at a specified frequency and peak to peak (p-p) displacement amplitudes. A few investigations on the dynamic radial and axial stiffnesses using different frequencies and peak to peak amplitudes have been performed.

To specify the test configuration, the frequencies selected were the operating frequency of the main excitation source of compressor which is approximately 47 Hz. By measuring the excitation response using accelerometer, it is shown in Figure 16 that the maximum excitation can go up to about 0.078 mm. The frequency of 25 Hz is an additional frequency to investigate the stiffness at this excitation level. For the dynamic displacement amplitude, peak-to-peak (p-p) amplitudes of 0.08, 0.5 and 2 mm have been applied for the tests. Tables 5 and 6 show the test configuration and its corresponding dynamic radial and axial stiffnesses obtained.

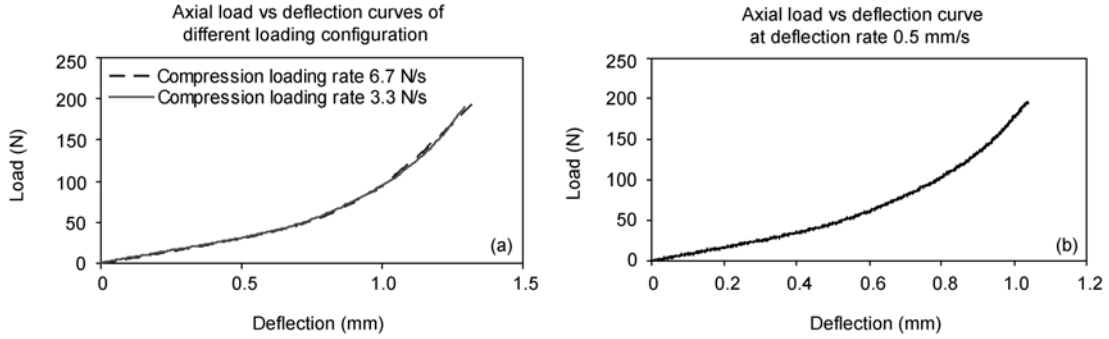

Figure 15 Axial load-deflection curves at (a) different loading rates and (b) deflection rate 0.5 mm/s.

Table 5 Dynamic radial stiffness of rubber grommet

Sample No.	Test configuration		Dynamic radial stiffness (N/mm)
	Frequency	Peak-to-peak amplitude	
1	25	0.08	54.41
2	47	0.08	58.23
3	25	0.5	43.71
4	47	0.5	45.75
5	25	2	30.92
6	47	2	31.25

Table 6 Dynamic axial stiffness of rubber grommet

Sample No.	Test configuration		Dynamic axial stiffness (N/mm)
	Frequency	Peak-to-peak amplitude	
1	25	0.08	250.71
2	47	0.08	263.34
3	25	0.5	171.23
4	47	0.5	177.81
5	25	2	116.24
6	47	2	118.30

Figures 17 and 18 show the radial and axial dynamic stiffnesses in graphical plots.

Based on the results, the grommet is stiffer in dynamic condition than in static condition. The dynamic stiffness changes more significantly in crosshead p-p displacement than its frequency. When the p-p displacement is higher, the dynamic stiffness is inversely lower. Based on the measurement results, the dynamic stiffness measured at operating frequency of 47 Hz and p-p displacement of 0.08 mm are applied in the suction tube assy and discharge tube assy model as axial and radial stiffness (k_a, k_{r1}, k_{r2}) representations of both the tubes mounting to the compressor side. The acquisition for axial and radial stiffnesses (k_a, k_{r1}, k_{r2}) mounting to the compressor which were unknown variables previously is now fulfilled. The stiffness variables for the tube ends mounting to the condenser coil are applied to fine tuning practice in the numerical model based on correlation with impact hammer test results.

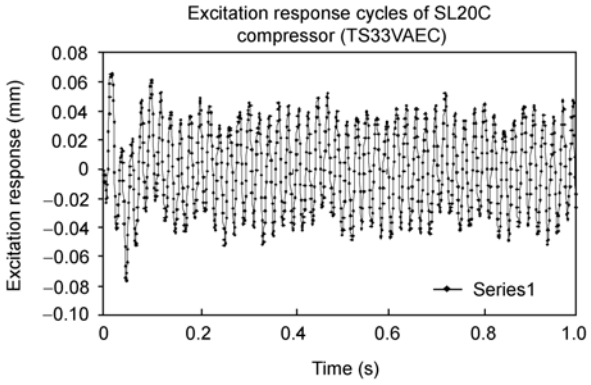

Figure 16 Excitation response of compressor with maximum displacement of about 0.078 mm.

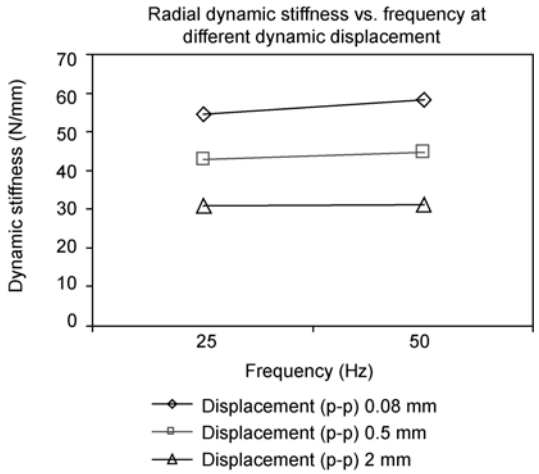

Figure 17 Radial dynamic stiffness of grommet at different dynamic displacements and frequencies.

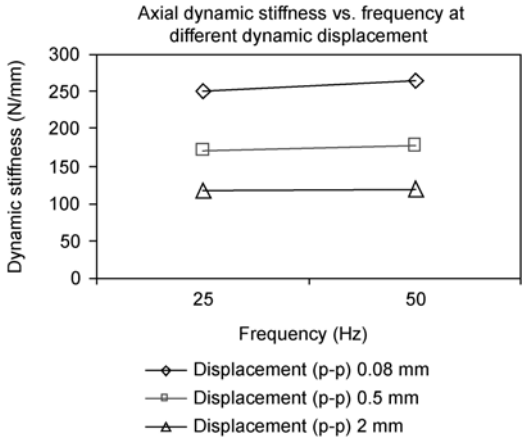

Figure 18 Axial dynamic stiffness of grommet at different dynamic displacements and frequencies.

3.4 Simulation results

After the spring stiffness is defined on the models, the mode shapes and natural frequencies of the structures are extracted. The fundamental and first two harmonics (second and third) modes of both the piping models are axial bending modes. Figure 19 shows the simulated first six mode shapes of the suction tube assy. Mode 1 and mode 2 of the suction tube assy are a typical front-back axial bending and a side axial bending modes at low frequency of 6.71 and 7.09 Hz respectively. The third mode consists of front-back axial bending with slight up and down tilted displacement. Modes 4, 5 and 6 are different rotational modes which occur at higher frequencies. Meanwhile, the pipe end connecting to compressor of the discharge tube assy moves axially at 6.62 Hz in the first mode while the other ends have very low displacements as they are mainly stiffer and constrained. From mode 2 to mode 6, the tube mainly moves in a combination of axial and rotational modes at different frequencies ranging from 8.31 to 23.45 Hz. The simulated first six mode shapes of the discharge tube assy are shown in Figure 20.

4 Comparison of measured and simulated modal parameters

The comparison of measured and simulated modal properties of suction tube assy and discharge tube assy are tabulated in Tables 7 and 8 below. For the suction tube assy, both the measured and simulated natural frequencies are overall in good correlation with a maximum correlation error of 8.54% occuring at measured frequency of 29.5 Hz. For the frequency range from 0 to 200 Hz, it is found that the FE simulation extracts more natural frequencies than measured natural frequencies. The measured frequency of 179 Hz is not captured in simulation whereas the other four simulated frequencies at 7.09, 19, 131.68 and 197.51 Hz are not discovered from the modal testing. For the discharge tube assy, a maximum correlation error of 19.14% occurs at 13.48 Hz and there are about five natural frequencies where

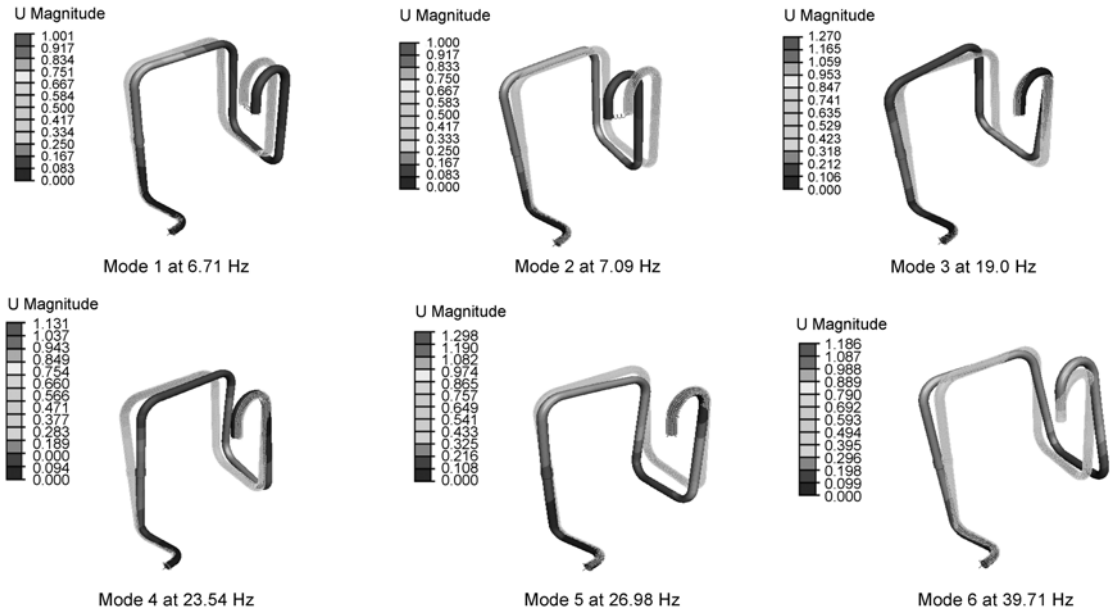

Figure 19 Simulated first six modes of suction tube assy.

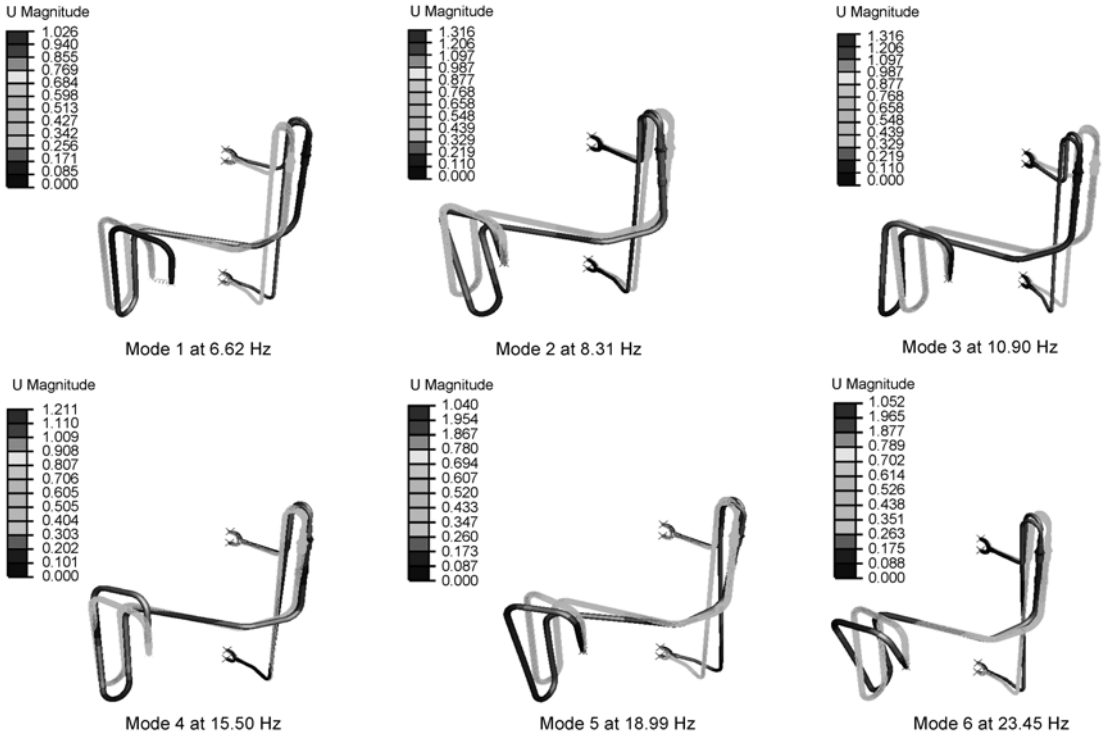

Figure 20 Simulated first six modes of discharge tube assy.

the correlation and comparison could not be determined. Some of the frequencies found in measurement are not found in simulation and vice versa. Nevertheless, the overall comparison of most of the frequencies gives a good degree of correlation with all existing comparison giving less than 20% error.

The phenomenon of miscorrelation and high correlation error between empirical and numerical approaches is always a main interest in this study. One of the reasons contributing to this problem is the measurement accuracy. Some natural frequencies appear within a very close frequency range where measurement may not able to capture the frequency

Table 7 Measured and simulated vibration characteristics of suction tube assy

Mode	Experiment		FEM	Error (%)
	Frequency	Damping ratio	Frequency	
1	6.33	2.55	6.71	+6.00
	-	-	7.09	-
	-	-	19	-
2	24	2.92	23.54	–1.92
3	29.5	2.86	26.98	–8.54
4	39	0.58	39.71	+1.82
5	48	0.15	46.05	–4.06
6	54	0.75	57.7	+6.85
7	77	2.51	77.56	+0.73
8	93	1.48	93.28	+0.30
9	117	0.64	119.04	+1.74
	-	-	131.68	-
10	155	0.92	155.86	+0.55
11	179	1.44	-	-
	-	-	197.51	-

Table 8 Measured and simulated vibration characteristics of discharge tube assy

Mode	Experiment		FEM	Error (%)
	Frequency	Damping ratio	Frequency	
1	6.68	2.70	6.62	–0.90
2	9.06	1.50	8.31	–8.28
3	13.48	1.17	10.90	–19.14
4	15.41	1.12	15.53	+0.78
5	17.70	0.79	18.99	+7.29
6	24.82	1.41	23.45	–5.52
7	27.31	1.86	25.61	–6.22
	-	-	31.48	-
8	42.16	0.63	41.75	–0.97
9	44.51	0.76	-	-
10	56.70	0.77	61.59	+8.62
11	65.37	0.94	63.89	–2.26
12	68.91	1.55	77.88	+13.02
13	85.05	0.56	88.09	+3.57
14	95.35	0.88	90.68	–4.90
15	116.18	0.61	-	-
16	149.22	0.40	135.08	–9.48
	-	-	138.60	-
17	174.06	0.31	180.74	+3.84
18	185.30	0.60	182.72	–1.39
19	192.30	-	-	-

response peak in a distinct form.

By comparing the measured and simulated mode shapes of the suction tube assy in Figure 21, the first three measured mode shapes are front-back dominant mode with mode 2 consisting of low side axial displacement. Mode 1 obtained from experiment is comparable with the one from simulation as both have axial front-back displacement at this mode. Measured mode 2 and mode 3 of suction tube assy are slightly different from the corresponding simulated modes 2 and 3. This can be seen when the simulated mode 2 is

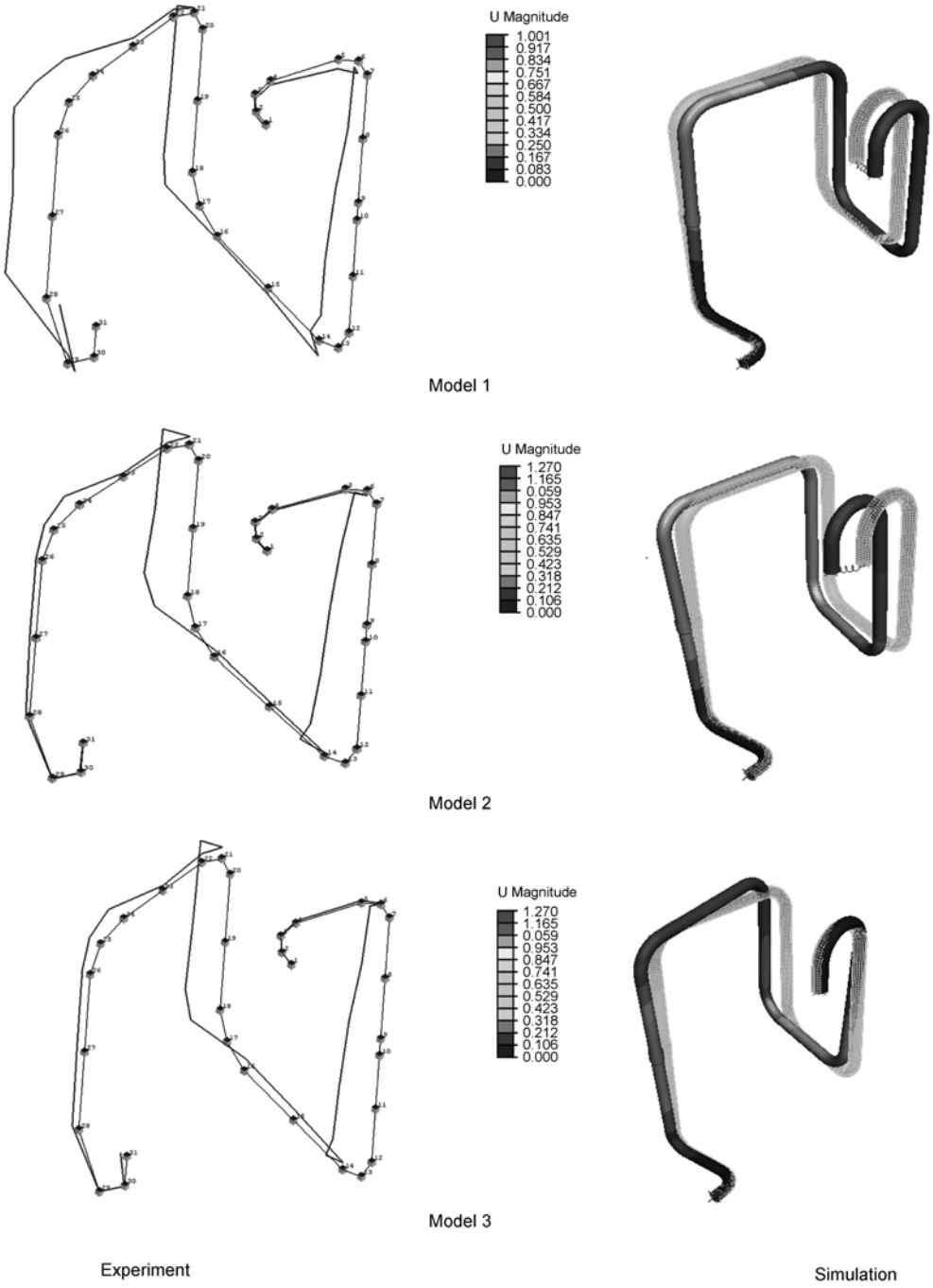

Figure 21 Comparison of three experimental and simulated mode shapes of suction tube assy.

mainly displaced along the side axial direction whereas measured mode 2 is a combination of front-back axial displacement and side axial displacement. The third simulated mode is displaced along front-back mode and tilted upward at the right side while the front-back mode is obvious in experimental data.

For discharge tube assy mode shapes comparison in Figure 22, both the simulated and measured first modes achieve agreement to each other. Both are displaced axially with the U-bend region moving in the front-back direction. The simulated and measured displacements of the second and third modes move axially with the U-bend region of the FE model swinging forward and backward for the second and third modes respectively.

5 Discussion and conclusion

The vibrational characteristics of the piping structures in air conditioner outdoor unit have been investigated by

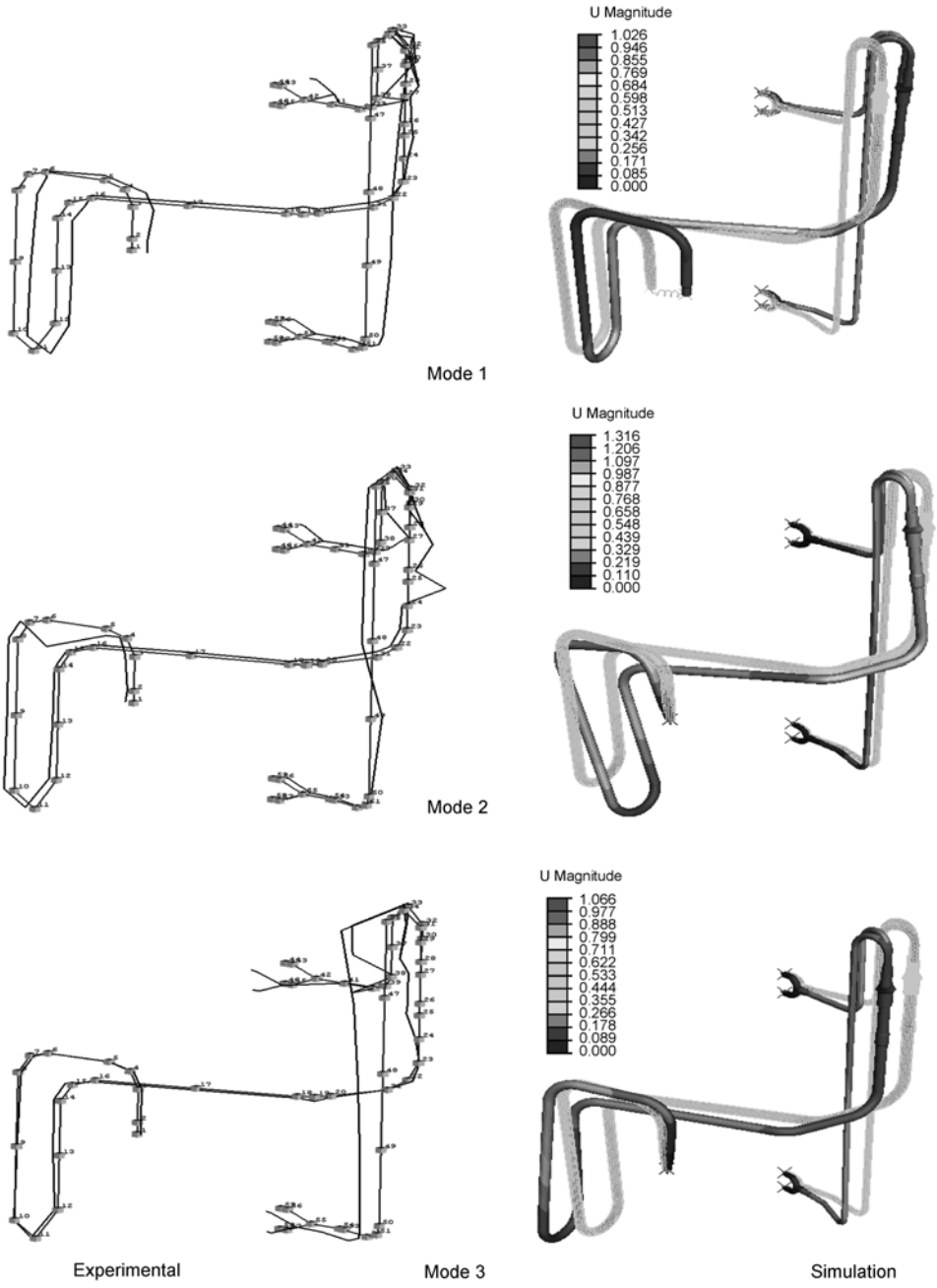

Figure 22 Comparison of three experimental and simulated mode shapes of discharge tube assy.

performing an impact hammer test. A numerical FE model is set up to correlate with the measured results. The main focus of this work is to investigate the dynamic stiffness of compressor-piping mounting for the vibration behaviour determination in the FE approach. The dynamic stiffness of compressor-piping mounting is represented by the dynamic stiffness of rubber grommet sitting beneath the compressor. This characterization reduces the initial 6 translational stiffness of both elastic end supports to 3 unknown stiffness variables at the other end of the tube mounting to valve at chassis. Parameter fine tuning is applied to obtain better correlation with experimental data.

Based on the grommet stiffness characterization test, the radial and axial stiffnesses are of rate dependant behavior and increase when the rate of deformation increases. The grommet is stiffer in dynamic condition than in static condition. When the frequency is higher, the dynamic stiffness will be correspondingly higher. It is found that the dynamic stiffness changes more significantly in crosshead peak-to-peak (p-p) displacement than its frequency. When the p-p displacement is higher, the dynamic stiffness is inversely lower. This is because the higher force induced has basi-

cally become dominant and overcomes the material resistant. Hence, the dynamic stiffness will be relatively low. The obtained 3 translational stiffnesses (k_a, k_{r1}, k_{r2}) are applied to the FE model as compressor-piping mounting stiffnesses. Hence, this locked down the translational stiffness of the compressor-piping elastic end support, leaving translational stiffness of the chassis-piping elastic end support to be investigated by fine tuning.

Based on the comparison between the numerical and experimental data, a reasonably good degree of correlation has been achieved especially on the natural frequency of the piping structures. The maximum error of approximately 8.5% and 19% occur on suction and discharge tubes respectively. Discrepancies occur between simulation and measurement results especially on natural modes. One of the reasons contributing to this problem is the measurement accuracy. Some natural frequencies appear within a very close frequency range where measurement may not able to capture the frequency response peak in a distinct form. Besides, the hit on all impact points may not be consistent and may not generate single impulse and sufficient energy to give appropriate natural mode of the structure.

The chassis-piping mounting characterization shall be studied and explored to investigate the elastic support stiffness under dynamic condition. A thorough work to study the characterization is necessary so that the parameter fine tuning can be substituted. Besides, the rotational stiffness of the elastic support is not considered in the FE model. The rotational effect is neglected in this work hence the natural modes and frequencies involving rotational DOF may not be correlated well with the measured ones. The rotational stiffness especially compressor-piping mounting support may play significant effect as it is subjected to rotational excitation by the rotary compressor.

The effect of centre of mass of compressor can be investigated in the FE model in comparison with the point mass modeling at the pipe end. The location of centre of mass shall give particular effect on the characteristics especially the low frequency range.

1 LMS International. The LMS Theory and Background Book. Leuven, 2000
2 Chuan X D, Guang M. Determining the boundary conditions by estimating RDOFs CMS for piping system. J Build Environ, 2007, 42: 2660–2666
3 Wang X H, Xu B, Redekop D. FEM free vibration and buckling analysis of stiffened toroidal shells. J Thin-Wall Struct, 2006, 44: 2–9
4 Pan Z, Li X B, Ma J J. A study on free vibration of a ring-stiffened thin circular cylindrical shell with arbitrary boundary conditions. J Sound Vib, 2008, 314: 330–342
5 Abaqus Inc. Abaqus Analysis User's Manual Version 6.8, Providence, 2008
6 Nitin S G, Sanjay S D, Sanjeev V B, et al. Practical Finite Element Analysis. India: Finite to Infinite, 2008
7 Rubber Development Inc. Technical Standard Website. http://www.rubberdevelopment.com/pages/eload.htm
8 Chew B. Dynamic data to predict response of elastomeric isolators. E.A.R Tech White Papers, 2003